Discriminating the States of Matter in Metallic Nanoparticle Transformations: What Are We Missing?

John M. Pettibone,* Julien Gigault,* and Vincent A. Hackley

Materials Measurement Science Division, National Institute of Standards and Technology, Gaithersburg, Maryland 20899, United States

ABSTRACT A limiting factor in assessing the risk of current and emerging nanomaterials in biological and environmental systems is the ability to accurately detect and characterize their size, shape, and composition in broad product distributions and complex media. Asymmetric flow field-flow fractionation (A4F) is capable of separation without stationary phase interactions or large applied forces. Here, we demonstrate unprecedented A4F fractionation of metallic nanoclusters with core diameters near 1 nm and with high resolution. The isolated nanocluster populations were characterized online with UV—vis absorption and inductively coupled plasma mass spectrometry (ICP-MS). We apply our methodology to a model system, poly(*N*-vinyl-2-pyrrolidone)-protected silver nanoparticles with an excess of tripeptide—glutathione (GSH). The temporal evolution of the initial silver nanoparticle distribution in the presence of excess GSH results in the appearance and persistence of a continuum of matter states (*e.g.*, Ag^+ nanoclusters and nanoparticles) that could be fractionated with A4F, characterized by their optical signatures and diffusion coefficients, and quantified with ICP-MS. The results suggest that our methodology is generally applicable to metallic systems when appropriate online detection is coupled to the A4F. Because we extend the capability of the coupled A4F system to reliably detect, characterize, and quantify metallic populations in the sub-5 nm regime, the opportunity exists to survey the formation and transformation products of nanomaterials in more relevant biological and environmental systems. Thus, individually assessing the risks associated with specific ion, nanocluster, and nanoparticle populations is achievable, where such populations may have previously been misrepresented.

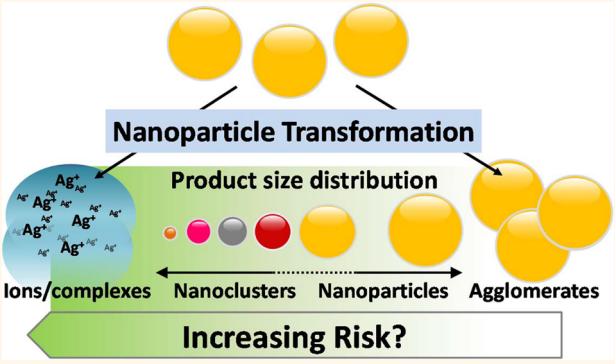

KEYWORDS: nanocluster · field-flow fractionation · silver · dissolution · synthesis · nanotoxicology · nanomaterials

Development of new nanomaterials and more efficient synthetic procedures for controlling composition, shape, and size of materials on the atomic scale is increasing rapidly. The ability to efficiently characterize the formation and transformation processes of these materials is of fundamental importance, resulting in more efficient syntheses and will allow more rapid risk assessment through increasingly accurate models. The development of new methodologies is necessary to meet the needs of the broad nanoscience community for detecting and determining the distribution of size, shape, and composition over the entire nanolength scale.

Silver nanoparticles (AgNPs) are the most widely incorporated metal nanomaterial in consumer products,[1] which is expected to result in the accumulation of silver in environmental systems. Because of their extensive use, a large body of work examining the stability, transformation, and toxicity is present in the literature and has recently been reviewed.[2−5] Transformation of silver nanoparticles into Ag^+ and subsequent reduction to form progeny nanoparticles has been demonstrated on surfaces,[6] in biological systems,[7] and in environmental systems,[8] indicating complex pathways for processing and formation that are sensitive to environmental conditions (*e.g.*, *hν*, complexing agents, oxidants, pH, *etc.*). The toxicological response induced from the introduction of AgNPs to microbial or human cell models has generally been framed into either a nanoparticle or ion response and has been previously summarized,[9−11]

* Address correspondence to john.pettibone@nist.gov, julien.gigault@nist.gov.

Received for review December 18, 2012 and accepted February 20, 2013.

Published online February 20, 2013
10.1021/nn3058517

where nanoparticle-induced responses are reportedly a function of capping agent, size, and shape. However, because multiple pathways for transformation and dissolution are known to exist, studies examining the potential presence of a continuum of matter states are necessary.

Commonly, nanoparticle transformation products, including those derived from dissolution, are characterized by the separation of "nanoparticle" and "soluble" fractions *via* different filtering techniques or centrifugation and quantified by elemental methods (*e.g.*, inductively coupled plasma mass spectrometry (ICP-MS) and atomic absorption spectroscopy). The efficiency of these methods and the distribution of metal states (ions, nanoclusters, nanoparticles, agglomerates/aggregates) in the filtrate are not extensively characterized, resulting in possible ambiguity in the relationships between cause and effect reported in environmental and biological systems. Small nanoparticles (<3 nm) and metallic nanoclusters stabilized with ubiquitous environmental and biological capping agents have been synthesized in the laboratory but, to the best of our knowledge, have not been extensively surveyed as nanoparticle transformation products.

Metallic nanoclusters (*e.g.*, Au, Ag, Cu, CdSe, *etc.*) are the matter bridging bulk metals and organometallic complexes. They inherently possess distinct electronic, catalytic, optical, and magnetic properties.[12−16] Nanoclusters are formally defined as molecular species with both distinct electronic states and known stoichiometry. Furthermore, because the properties of metallic nanoclusters are known to be size-dependent, it is reasonable to surmise their interaction with environmental and biological systems will also be size- (nuclearity) and capping-agent-dependent.[17,18] However, the impacts of metallic nanoclusters in environmental and biological systems are not well-established, and their presence may be completely overlooked in studies employing characterization methods with insufficient isolation and identification tools or detection limits. To better discriminate the effects from distinct metallic species, including ions, nanoclusters, nanoparticles, agglomerates, and aggregates, instruments and validated methods capable of detecting and characterizing the entire product distribution in complex media are needed.[19]

Tools used for monitoring and quantifying nanomaterial formation and transformation are broad. Electron microscopy is commonly used to examine the size and shape of species present in solution but is not statistically reliable for probing the full product distribution. Liquid chromatography (LC) techniques, including size exclusion chromatography (SEC), recycling SEC, high-performance LC (HPLC), and reverse-phase HPLC, have been successfully applied for separating nanoparticle and nanocluster species.[20−25] However, known limitations with these chromatographic techniques are inherently present, resulting from column packing, enthalpic interactions with the stationary phase, sample deterioration, or use of high ionic strength media (commonly used in SEC) that can affect the analyte distribution.

Analytical ultracentrifugation (AUC) has been used to separate a broad range of materials based on their sedimentation and diffusion coefficients and is capable of separating size, shape, and density without the stationary phase interactions.[26,27] A limitation for AUC is that detection is limited to optical absorbance, requiring further offline measurements for determining composition, quantification of species with unknown molar absorption coefficients, ε, and for following nanoparticle transformation in complex media. Also, morphological changes to samples such as agglomerates can occur in the large applied field.

Asymmetric flow field-flow fractionation (A4F) coupled to appropriate online detectors has the ability to fractionate samples based on size, shape, and composition online in complex media with minimal sample perturbation.[28,29] The absence of enthalpic interactions with a stationary phase common in other chromatographic techniques, and the ability to minimize interaction of the analyte and the "soluble fraction", which includes free ions, free ligands, metal−ligand complexes, *etc.*, *via* a focusing step prior to elution, minimizes sample preparation requirements. These advantages are attractive for monitoring and characterizing both formation and transformation processes in synthesis procedures and in biological and environmental matrices, but some *a priori* knowledge, such as optical signatures or stoichiometry, may be necessary for confident assignment with the coupled detectors (*e.g.*, diode array detector (DAD), light scattering, fluorescence, mass spectrometry, *etc.*). The large parameter space for optimizing fractionation (*e.g.*, cross-flow, main flow, membrane composition, pH, mobile phase, channel geometry, *etc.*) and the sensitivity of the fractionation of each parameter in the A4F has been a possible limitation in the widespread use of A4F for monitoring metallic nanoparticle transformations in environmental and biological systems. For example, coupled A4F systems have previously been used to examine AgNP transformation, but fractionation by size has been limited to species $\geq$10 nm.[30−32] Therefore, until now, the ability to selectively identify and characterize smaller metallic species with coupled A4F systems has not been demonstrated.

In the current study, we first demonstrate the generally applicable and unprecedented A4F fractionation of sub-10 nm metallic species using previously characterized Ag nanoclusters, where the smallest population of nanoclusters has metallic core diameters $\approx$1 nm. The nanoclusters are characterized online with UV−vis absorption, light scattering, and ICP-MS. We apply the optimized conditions to a model system, polymer-protected AgNPs, in the presence of excess concentrations of a ubiquitous tripeptide to probe the continuum of

products present during the AgNP transformation in aerobic environments with coupled A4F and ICP-MS. The resulting product distributions display a continuum of sizes that persist in solution and can be fractionated and quantified online. The identification of a continuum of products from transformation processes indicates that categorizing the effects observed into nanoparticle and ion categories may be misrepresentative and possibly inaccurate.

RESULTS AND DISCUSSION

GSH-Protected Silver Nanoclusters. Characterization of small silver species has been more difficult than other metallic systems (*e.g.*, gold) due to the lack of analytical techniques for probing the entire product distribution and due to the inherent oxidative instability for Ag^0. Furthermore, many existing analytical tools for determining the size distribution, especially in the smallest size regimes of metal−ligand complexes, "molecular" nanocluster species, and small nanoparticles, generally require extensive sample processing (*e.g.*, purification) or have limiting concentration requirements. A4F, in general, is less limited by sample concentration requirements and does not typically require undesired processing because the sample is "focused" and separated prior to elution (unlike traditional chromatographic techniques). Until now, the fractionation of very small (<5 nm) metallic nanoparticles and nanoclusters using A4F has not been demonstrated in the literature, but we clearly show that the resolution and selectivity are sufficient to probe a large continuum of sizes.

We first demonstrate the ability to detect and identify small GSH-protected nanoclusters with previously reported core sizes[33] using the coupled A4F comprising UV−vis, DLS, and ICP-MS detection to demonstrate the high-resolution capability of the system. To ensure that only small silver nanoclusters were prepared, a greater than 4:1 molar ratio of $[AgNO_3]$/[GSH] was used in the synthesis procedure at 0 ± 1 °C. The bulk UV−vis spectra for the silver nanocluster standards at t = 20 min and t = 24 h are presented in Figure 1, where t represents the time after resuspension of the dried sample in water. At t = 20 min, the UV−vis spectrum contains a single broad band centered near 472 nm, indicating that only small nanoclusters are present in the solution based on previously reported optical signatures and supported by light scattering measurements (*vide infra*). We also examined the nanocluster standards qualitatively with transmission electron microscopy (TEM) and observed no large silver species present (not shown).

Because the larger GSH-protected silver nanoclusters are reportedly less stable in solution relative to their smaller counterparts,[33] we allowed the larger nanoclusters to dissolve in the presence of ambient conditions and fluorescent light for 24 h. At t = 24 h, the resulting bulk UV−vis spectrum exhibits an absorption maximum at 487 nm with a less intense absorbance band centered near 400 nm, which is consistent with the loss of larger nanoclusters containing ≳30 Ag atoms.[33] The bulk UV−vis spectra support the sole presence of GSH-protected silver nanoclusters after the dried sample is initially suspended and the persistence of only small, more stable nanoclusters after 24 h.[33−35] This nanocluster distribution represents an ideal standard for examining selectivity of the coupled A4F-ICP-MS in a system containing small metallic species with diameters <5 nm.

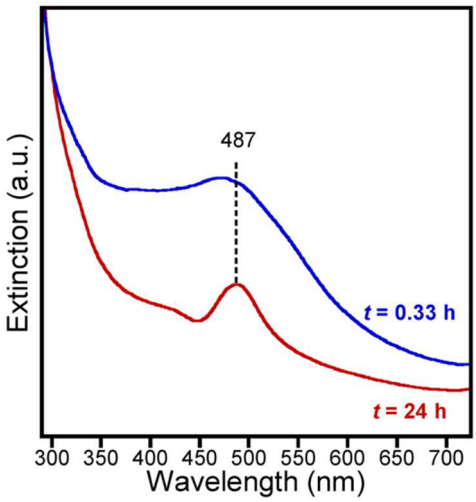

Figure 1. Batch UV−vis spectra of the resuspended GSH-protected Ag nanoclusters at two time points in DI water: immediately after suspension, t = 0.33 h (blue, top) and at t = 24 h (red, bottom). At 24 h, signatures for larger Ag nanoclusters are absent, indicated by the narrowing of the initial broad absorbance and the decrease in baseline intensity. The absorbance at 487 nm becomes the salient feature accompanied by a weaker absorbance centered near 400 nm, which is characteristic of the previously reported optical signatures for smaller GSH-protected nanoclusters containing ≲30 Ag atoms.

Results for the GSH-protected Ag nanocluster solutions fractionated with our optimized A4F conditions (Table 1, condition 1) are presented in Figure 2. At t = 0.33 h (Figure 2A), two distinct peaks are observed in the 254 nm trace (red trace) with retention times, t_R, at 4.15 and 5.61 min and denoted peak 1 and peak 2, respectively. Equation 1 in the Materials and Methods section can be used to calculate the diffusion coefficient of each species, and the hydrodynamic diameter, D_H, is approximated based on the Stokes−Einstein equation in an applied flow field.[36] The two fractionated peaks likely contain a distribution of nanoclusters with similar diffusion coefficients, indicating an average calculated D_H. Applying eq 1 yields D_H of 1.8 and 2.5 nm for peaks 1 and 2, respectively. The calculated 1.8 nm D_H of the nanocluster population in peak 1 is similar to the reported crystal structure diameter of $[TOA^+][Au_{25}(SCH_2CH_2PH)_{18}^-]$, which has a metal core

TABLE 1. A4F Conditions Used for Separation with the PES Membrane

	detector flow, $\dot{V}_{out}$, (mL min^{-1})	cross-flow, $\dot{V}_{cr}$ (mL min^{-1})	spacer height (μm)	channel height[a] (ω, μm)	mobile phase composition
condition 1 (cluster separation)	0.5	0.8	490	330	0.5 mmol L^{-1}, NH_4NO_3, pH 6.8
condition 2 (nanoparticle separation)	0.5	2.0	350	280	0.5 mmol L^{-1}, NH_4NO_3, pH 6.8

[a] Calculated based on a 3 nm gold standard under the same conditions.

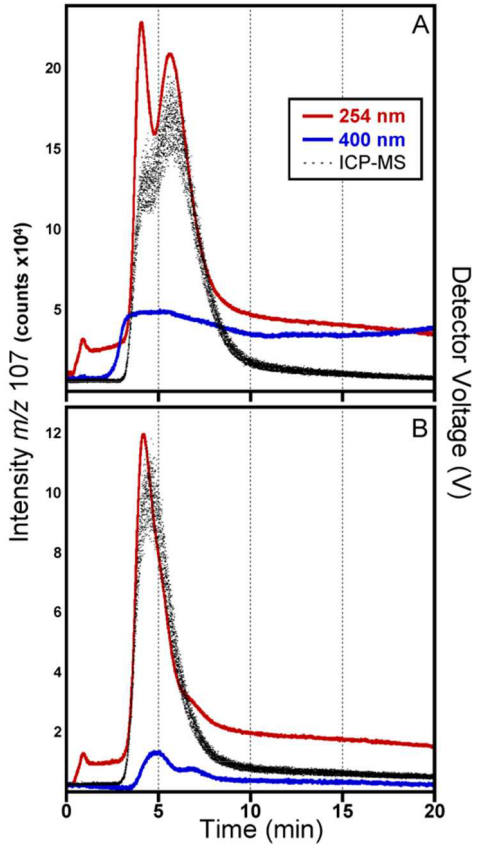

Figure 2. Fractograms of GSH-protected silver nanoclusters at (A) t = 0.33 h and (B) t = 24 h after resuspension in DI water examined with condition 1. At t = 24 h, the diminished intensity of peak 2 at t_R = 5.61 min represents the loss of larger, less stable nanoclusters and the persistence of small nanoclusters comprising ≲30 Ag atoms in peak 1 at t_R = 4.15 min.

diameter of ≈1 nm stabilized by a ligand shell.[37,38] In the 400 nm trace (blue trace), a single broad band is present. However, because the nanoclusters have distinct optical signatures with differing ε, the single wavelength traces may not be sufficient for relative quantification or detection of the individual species present and highlight the need for further online detection.

Examination of the m/z 107 ICP-MS signal intensity (black dots) provides information regarding the Ag mass distribution and clearly separates the void time, t^0, at ≈0.8 min from the slower eluting Ag species. A majority of the Ag mass distribution observed in the fractogram is found in peak 2, but two populations of silver species are clearly resolved. Further qualitative size information can be derived from the relative intensity of online DLS signals. Although similar signal intensities for peak 1 and peak 2 are observed with ICP-MS, only a discernible DLS signal is only observed corresponding with peak 2 and qualitatively indicates the presence of more efficient scatters (larger nanoclusters) compared to the Ag population in peak 1. However, there was insufficient scattering intensity for size determination even at increased nanocluster concentrations (data not shown), further supporting the presence of small Ag species. The UV–vis, ICP-MS, and light scattering data support the presence of only small silver species and are consistent with the bulk UV–vis spectrum in Figure 1.

At t = 24 h, the maximum peak intensities observed with the 254 nm trace and ICP-MS signal shift to shorter t_R values (Figure 2B). In the 254 nm trace, peak 1 at 4.18 min remains after 24 h, but only a small shoulder is observed centered near 6.6 min. Similarly, the 400 nm trace displayed two distinct peaks. The Ag mass distribution observed from ICP-MS corresponds almost completely with peak 1. Furthermore, the maximum m/z 107 intensity of peak 1 was similar at t = 0.33 and 24 h, indicating the preservation of the smaller nanocluster population. After 24 h, no observable signal is observed from DLS, which further supports evidence for the loss of the larger silver species.

Combining data from the bulk UV–vis absorbance for the previously reported, well-characterized nanoclusters and the A4F-UV–vis-DLS-ICP-MS results, the clear separation of two distinct populations of nanoclusters is observed, where peak 1 represents clusters containing ≲30 Ag atoms and peak 2 represents larger nonplasmonic Ag species based on previous mobility measurements.[33] The nanocluster samples were also examined with coupled A4F after processing with a 0.02 μm filter to investigate its ability to distinguish ions from nanocluster standards. The distribution observed under condition 1 was unchanged after filtration, indicating that the 0.02 μm filter used does not distinguish between Ag^+ species and small nanoclusters. However, further work will be necessary to develop sufficient separation methods. The data collectively provide clear evidence for the separation performance of very small silver species with A4F and provide a tool for examining more complex systems.

Application of Methodology to PVP-Coated AgNP Transformation. Data in the previous section clearly demonstrate the selectivity of A4F in the heterogeneous silver nanocluster solutions. Here, we provide further data

that establish the effectiveness of the current methods for examining the transformation of an environmentally relevant model, PVP-protected silver nanoparticles in the presence of GSH. In this size regime, the environmental community has lacked reliable tools for probing and differentiating the full size distribution, resulting in common practices that separate nanoparticles and the "soluble" fraction through filtering techniques. We clearly show that a continuum of silver states (*e.g.*, ions, clusters, nanoparticles, and aggregates) is present during the transformation, which can be distinctly identified with the currently described method.

The fractograms obtained with the coupled A4F system for the synthesized PVP-coated AgNPs in the absence of GSH under condition 2 are presented in Figure 3A. The solution was filtered, resuspended, bath sonicated, and filtered again with a 100 kDa filter to remove free PVP and Ag^+ species present in the stock solution. The optical signatures of the nanoparticles are clearly separated from t^0, and the 254 and 400 nm traces overlap with $t_R \approx 9.9$ min. The maximum absorbance was observed with the 400 nm trace, representative of the plasmonic character of the silver nanoparticles. The *m/z* 107 peak intensity corresponds with the onset of the observed intensity increase of both 254 and 400 nm traces, indicating that the silver is present only in nanoparticle form and is characteristic of a NP distribution. The mode *z*-average D_H for the filtered sample measured online and offline with DLS was 25 ± 1 nm. The full width at half-maximum standard deviation across the peak observed online was ±4 nm.

At $t = 80$ min after the addition of ≈100 times molar excess of GSH to the PVP-AgNP stock solution (Figure 3B), two peaks appear in the 254 nm trace. Peak 1 coincides with t^0 and is not suitable for size determination. An observed shift in t_R for peak 2, which corresponds to the AgNPs, is now observed at 7.3 min, representing a D_H of 15 nm that was statistically the same based on t_R and online DLS. The *m/z* 107 peak signal intensity parallels the UV−vis traces, and a large fraction of the silver is contained in peak 1. The peak shift suggests strong interaction between GSH with the PVP-coated AgNPs. Because PVP is known to stabilize numerous Au nanocluster nuclearities[39] and is reported to be retained during sulfidation of AgNPs,[40] further investigation on the role of PVP during dissolution of specific silver species (sizes) is necessary to elucidate the transformation mechanism, which is currently ongoing.

At 24 h, peaks that were unable to be resolved at $t =$ 80 min become increasingly separated from t^0. At $t =$ 4 days, a distinct peak at $t_R = 2.88$ min is observed in both the 254 and 400 nm traces. A concomitant increase in the *m/z* 107 signal intensity is observed with the shift of t_R for the fastest eluting peak, indicating the appearance of small Ag products. Because the ratio between t_R and t^0 is too small to accurately determine the diffusion coefficient, further optimization is necessary.[41]

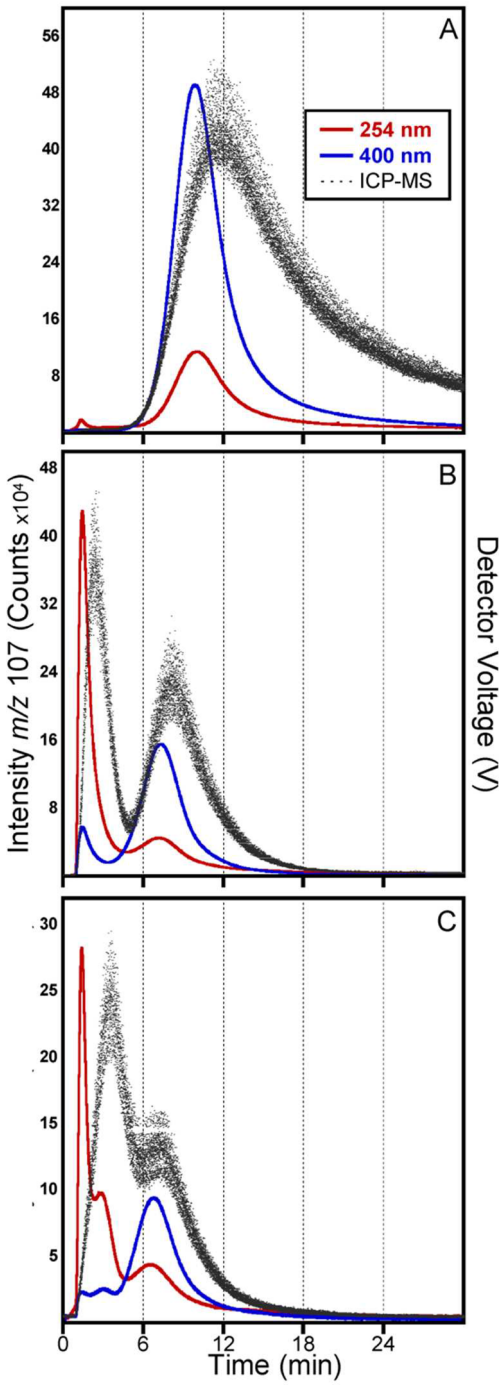

Figure 3. (A) Fractogram for the PVP-protected AgNP stock solution in the absence of GSH monitored at two wavelengths, 254 nm (red trace) and 400 nm (blue trace), and silver was monitored by the *m/z* 107 intensity (black dots) online with a coupled ICP-MS. The increased absorbance at 400 nm relative to 254 nm is characteristic of silver nanoparticles. Fractograms for the resulting silver populations in the presence of excess GSH at (B) $t = 80$ min and (C) $t = 4$ days. With increasing time, the original AgNP peak shifts to shorter t_R, indicating an increase in the diffusion coefficient and a decrease in D_H. Concomitantly, a large peak approaching t^0 appears after the addition of GSH; at $t = 4$ days, a peak at $t \approx 2.85$ min becomes separable from the overlapping t^0 and other small product peaks, but resolving different population sizes and measuring their diffusion coefficients cannot be determined under the current conditions. The fractograms represent the separation under condition 2.

Until now, further separation of a population of metallic species eluting near t^0, similar to the peak at t_R = 2.88 min in Figure 3C, has not been demonstrated, and thus calculated values for the size and product distribution were unreliable and inaccurate. Here, the demonstrated ability of the coupled A4F to fractionate silver nanoclusters with <30 atoms allows us to probe the entire metallic nanoproduct distribution in our model system.

Applying the A4F cluster conditions (condition 1) to the solution that has sufficient resolution for probing the smallest species results in the appearance of three distinct peaks (Figure 4B), which do not correspond to the AgNPs in Figure 3C and 4A (peak 2 in condition 2) and their diffusion coefficients determined using eq 1 in the Materials and Methods section. The 254 and 400 nm traces both clearly distinguish three populations of separable peaks with t_R at 3.5, 5.75, and 8.38 min, which correspond to 1.8, 2.5, and 5.5 nm diameters, respectively. Furthermore, the silver distribution measured online with ICP-MS also displays three distinct populations, consistent with the UV−vis traces. The largest *m/z* 107 signal intensity (peak 2) results from the ≈2.5 nm population. A DLS signal is observed, coincident with the UV−vis signals at 5.75 and 8.38 min, that is too weak for reliable size determination but which nevertheless confirms the presence of small silver nonplasmonic nanoclusters. The optical signatures of the clusters were also examined with the DAD detector, providing further evidence of the presence of silver nanoclusters. Furthermore, persistence of nanoclusters in solution was observed for more than 2 weeks in all samples, suggesting that the lifetime of these species is sufficient for many exposure scenarios.

Previous reports of nanocluster formation induced by ligand etching of gold and silver nanoparticles have been reported[15,42] but resulted from the etching of much smaller diameter (<5 nm) nanoparticles. Furthermore, engineered silver nanoclusters are known to persist when stabilized with other controlled peptide sequences and introduced for fluorescent cell labeling,[43] further suggesting that stable, adventitious nanoclusters are also likely to exist. The formation of silver nanoclusters resulting from the transformation of relatively large PVP-protected silver nanoparticles employed here obfuscates the formation pathway of the nanoclusters. The mechanism for nanocluster appearance is currently being investigated as well as nanoparticle processing in more environmentally relevant media.

Overall, we have demonstrated unprecedented separation capability of A4F in the sub-10 nm regime, which resulted in the identification of multiple populations of small nonplasmonic silver species in the model system. Because the physicochemical properties of ligated silver nanoclusters are size-dependent, we surmise that ecological and toxicological risks associated with these small species will also be size-dependent,

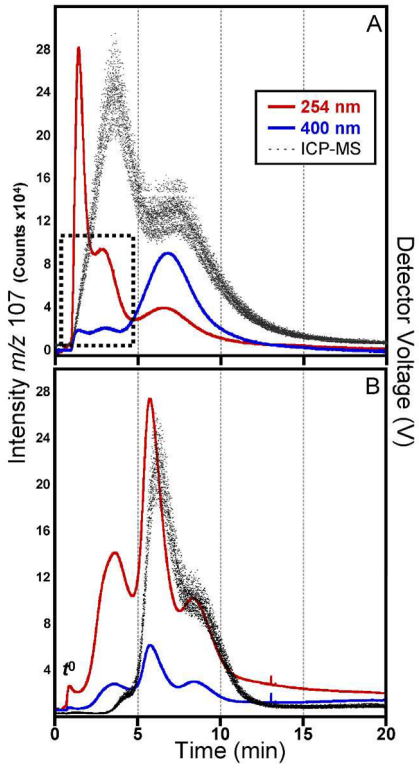

Figure 4. (A) PVP-AgNP solution at $t \approx 4$ days after excess GSH addition under condition 2 and (B) increased selectivity and resolution of the smallest silver species present with condition 1. Optimized conditions result in three distinct Ag populations that are sufficiently separated from t^0 at 3.5, 5.75, and 8.38 min corresponding to D_H of 1.8, 2.5, and 5.5 nm, respectively.

similar to reported studies on ligated Au nanoclusters.[17,18] The application of A4F to other metallic systems will require coupling to appropriate detectors and likely some knowledge of the product signatures, but the ability to fractionate the entire product distribution with high resolution is now validated. We believe the current data and methods will provide the impetus to reassess previous conclusions regarding the products, rates of processing, and risks of AgNPs in environmentally and biologically relevant systems.

CONCLUSIONS

By using well-characterized GSH-protected silver nanoclusters as size references, we have unequivocally demonstrated for the first time the ability of A4F to separate small metallic species (nanoclusters) with core diameters ≈1 nm and with high resolution, which was characterized online with UV−vis absorbance, DLS, and ICP-MS. Passing the silver nanocluster standard solution through a 0.02 μm filter resulted in almost no change in the peak shape or *m/z* 107 Ag intensity, indicating that this filter is not sufficient for separating dissolved species (*e.g.*, ions and metal−ligand complexes) from the GSH-protected Ag nanoclusters. The data from the transformation of the PVP-protected AgNP distribution in the

presence of GSH collected using condition 2 exhibited the formation of small metallic species, but the fractionation in the channel was insufficient for resolving individual populations. However, application of the optimized conditions for the smallest regime (condition 1) resulted in the fractionation of three distinct silver populations, and the data clearly represent the formation of nanoclusters that could be identified by their optical signatures and their t_R. The identification and persistence of the metallic continuum in the commonly uncharacterized sub-5 nm regime suggest that a similar product distribution may be present in environmental or biological systems that afford similar reactions. Because the coupled A4F-UV/vis-DLS-ICP-MS is sensitive enough to identify, characterize, and quantify species of this size, the opportunity to re-examine the full product distribution of metallic transformations in more relevant systems may provide further insight into the size-specific risks associated with individual populations of ions, metal−ligand complexes, nanoclusters, and nanoparticle species. Further studies are currently ongoing to elucidate the relationship between transformation and dissolution of other metallic nanoparticles and the mechanism of both appearance and persistence of nanoclusters.

MATERIALS AND METHODS

Materials. Silver nitrate ($AgNO_3$, >99%), glutathione (GSH), sodium borohydride ($NaBH_4$, granular, 99.99%), poly(*N*-vinyl-2-pyrrolidone) (PVP, 10 kDa), and sodium citrate ($Na_3C_6H_5O_7$, 99%) were purchased from Sigma Aldrich.[44] All chemicals were used without further purification.

Synthesis of GSH-Protected Ag Nanoclusters and PVP-Protected Ag Nanoparticles. GSH-protected Ag nanoclusters were prepared following a previously reported procedure.[33] Briefly, 21.9 mg (0.129 mmol) of $AgNO_3$ was dissolved in a round-bottom flask containing 25 mL of deionized (DI) water (>18 MΩ·cm) and mixed with a magnetic stir bar. Subsequently, 169 mg (0.55 mmol) of GSH was added and vigorously mixed. The solution was submerged in an ice bath and allowed to mix for 0.5 h. Next, 47.5 mg (1.26 mmol) of $NaBH_4$ was dissolved in 6.25 mL of chilled DI water and added dropwise to the $AgNO_3$−GSH solution under vigorous stirring; this resulted in a color change from white to pale yellow. The resulting solution was stirred for 1 h in the ice bath, yielding a final dark red solution. The clusters were precipitated with methanol. The solution was centrifuged for 10 min at 525 rad s^{-1}, the supernatant decanted, and fresh methanol added; the solutions were briefly placed in a bath sonicator to resuspend the clusters, and the process was repeated. After washing, the samples were placed under vacuum in a desiccator to dry overnight. The resulting powder was deep red. The UV−vis spectrum of the clusters immediately resuspended is representative of small GSH-protected clusters (Figure 1), and the cluster size was determined previously assuming similar mobility of GSH-protected silver clusters and known stoichiometric GSH-protected gold nanoclusters.[33,34] Further experiments were conducted on the synthesized Ag nanoclusters after being passed through a syringe-driven 0.02 μm Anotop filter.

PVP-protected AgNPs were prepared in manner similar to a previous method.[45] In 80 mL of boiling DI water, 5.1 mg (0.030 mmol) of $AgNO_3$ and 18 mg (0.07 mmol) sodium citrate were added and magnetically stirred. Next, 3.5 mg (0.090 mmol) of $NaBH_4$ dissolved in 1 mL of DI water was added dropwise to the boiling solution mixed at 125 rad s^{-1} and mixed for 15 min. The solution was cooled, and 100 mg of PVP was added and stirred overnight. The solution was covered with Al foil and stored in a refrigerator. Prior to use, the solution was washed and filtered with a 100 kDa centrifuge filter to remove excess reagents.

Instrumentation. The flow-mode analysis system comprises an Eclipse 3+ A4F (Wyatt Technology, Santa Barbara, CA), 1200 series UV−vis absorbance diode array detector (DAD) (Agilent Technologies, Santa Clara, CA), and a dynamic light scattering (DLS) detector (DynaPro, Wyatt Technology). Data from the above detectors were collected and analyzed using Astra software (version 5.3.1.18, Wyatt Technology). The A4F channel height, ω, was established using spacers of 350 or 490 μm. Information describing the calibration for AgNP under condition 2 was previously reported,[32] and information regarding the gold nanoparticle calibration standard used for condition 1 is found in the Supporting Information. The channel dimensions were as follows: 26.5 cm long and narrowing in width from 2.1 or 1.9 cm, to 0.6 cm, for the 350 or 490 μm spacer, respectively. Polyethersulfone (PES) 10 kDa membranes were purchased from Wyatt Technology and used in the A4F cell. Mobile phase flow is generated using a 1100 series isocratic pump (Agilent Technologies) equipped with a degasser (Gastorr TG-14, Flom Co., Ltd., Tokyo, Japan). Injections are performed using a manual injection valve (Rheodyne 7725i, IDEX Corporation, Oak Harbor, WA) equipped with stainless steel sample loops of different volumes. The A4F and associated detection chain is coupled to a model 7700x ICP-MS (Agilent Technologies) with a Micro Mist nebulizer for quantitative mass determination. Offline (batch mode) UV−vis absorbance measurements were performed using a Perkin-Elmer (Waltham, MA) Lambda 750 spectrometer. The uncertainty reported for the diameter measured offline by DLS (Malvern Zetasizer Nano ZS) is the standard deviation of five repeat measurements. The uncertainty of online DLS measurements is the standard deviation of the diameter values measured across each peak.

A4F Methodology. The condition for normal mode elution in A4F is generally defined as $t_R > 5t^0$, where t_R is the retention time and t^0 is the void time. Operating in this condition results in a relationship between the retention time and the diffusion coefficient such that

$$t_R = \frac{\omega^2}{6D} \ln\left(1 + \frac{\dot{V}_c}{\dot{V}_{out}}\right) \quad (1)$$

where ω is the effective channel height, D is the diffusion coefficient, and $\dot{V}_c/\dot{V}_{out}$ is the ratio of the volumetric cross-flow and detector flow rates. By applying the Stokes−Einstein equation in an applied flow field,[36] the hydrodynamic diameter, D_H, is calculated. Peaks that do not have sufficient separation from t^0 cannot be calculated within the theoretical constructs of normal mode elution. In this study, we optimized the method for high selectively for separation of two size regimes summarized in Table 1, corresponding to species with hard sphere diameters $\lesssim$6 nm and $\geq$10 nm. These are identified as condition 1 and condition 2, respectively. Further details on A4F methodology and theory can be found in the literature.[32,41]

Transformation of PVP-Protected AgNPs. The stock PVP-protected AgNP solution was filtered using a 100 kDa centrifuge filter, resuspended, bath sonicated for 1 min, and the process was repeated to remove any free ligands and small Ag species. To 800 μL ($\approx$0.0003 mmol) aliquots of filtered stock solutions was added 150 μL of a 10 mg mL^{-1} GSH stock solution (0.0325 mmol); the solution pH was adjusted to $\approx$7.0 with NaOH, and the final volume was adjusted to 1500 μL. The solutions were vortexed at a setting of 75 rad s^{-1} and covered with Al foil. Replicate dissolution studies of PVP-protected AgNPs and GSH were run, and all samples exhibited similar product distributions. We do not report uncertainty on the product distributions because we demonstrated the formation process and did not extensively study the rates of processing.

Conflict of Interest: The authors declare no competing financial interest.

Acknowledgment. The authors thank L. Nguyen for help with TEM, and J. Fagan for insightful comments.

Supporting Information Available: Online DAD spectra for the resuspended nanocluster solutions and characterization of the gold nanoparticle standard for determining ω are provided. This material is available free of charge *via* the Internet at http://pubs.acs.org.

REFERENCES AND NOTES

1. Consumer Products Inventory, the Project on Emerging Nanotechnologies, Woodrow Wilson International Center for Scholars; www.nanotechproject.org/inventories/consumer/ (Accessed December 2012).
2. Levard, C.; Hotze, E. M.; Lowry, G. V.; Brown, G. E. Environmental Transformations of Silver Nanoparticles: Impact on Stability and Toxicity. *Environ. Sci. Technol.* **2012**, *46*, 6900–6914.
3. Tolaymat, T. M.; El Badawy, A. M.; Genaidy, A.; Scheckel, K. G.; Luxton, T. P.; Suidan, M. An Evidence-Based Environmental Perspective of Manufactured Silver Nanoparticle in Syntheses and Applications: A Systematic Review and Critical Appraisal of Peer-Reviewed Scientific Papers. *Sci. Total Environ.* **2010**, *408*, 999–1006.
4. Wijnhoven, S. W. P.; Peijnenburg, W.; Herberts, C. A.; Hagens, W. I.; Oomen, A. G.; Heugens, E. H. W.; Roszek, B.; Bisschops, J.; Gosens, I.; Van de Meent, D.; *et al.* Nano-Silver—A Review of Available Data and Knowledge Gaps in Human and Environmental Risk Assessment. *Nanotoxicology* **2009**, *3*, 109-U178.
5. Nowack, B.; Krug, H. F.; Height, M. 120 Years of Nanosilver History: Implications for Policy Makers. *Environ. Sci. Technol.* **2011**, *45*, 1177–1183.
6. Glover, R. D.; Miller, J. M.; Hutchison, J. E. Generation of Metal Nanoparticles from Silver and Copper Objects: Nanoparticle Dynamics on Surfaces and Potential Sources of Nanoparticles in the Environment. *ACS Nano* **2011**, *5*, 8950–8957.
7. Liu, J.; Wang, Z.; Liu, F. D.; Kane, A. B.; Hurt, R. H. Chemical Transformations of Nanosilver in Biological Environments. *ACS Nano* **2012**, *6*, 9887–9899.
8. Yin, Y.; Liu, J.; Jiang, G. Sunlight-Induced Reduction of Ionic Ag and Au to Metallic Nanoparticles by Dissolved Organic Matter. *ACS Nano* **2012**, *6*, 7910–7919.
9. Yang, X.; Gondikas, A. P.; Marinakos, S. M.; Auffan, M.; Liu, J.; Hsu-Kim, H.; Meyer, J. N. Mechanism of Silver Nanoparticle Toxicity Is Dependent on Dissolved Silver and Surface Coating in *Caenorhabditis elegans*. *Environ. Sci. Technol.* **2011**, *46*, 1119–1127.
10. AshaRani, P. V.; Low Kah Mun, G.; Hande, M. P.; Valiyaveettil, S. Cytotoxicity and Genotoxicity of Silver Nanoparticles in Human Cells. *ACS Nano* **2009**, *3*, 279–290.
11. Xiu, Z.-m.; Zhang, Q.-b.; Puppala, H. L.; Colvin, V. L.; Alvarez, P. J. J. Negligible Particle-Specific Antibacterial Activity of Silver Nanoparticles. *Nano Lett.* **2012**, *12*, 4271–4275.
12. Lu, Y. Z.; Chen, W. Sub-Nanometre Sized Metal Clusters: From Synthetic Challenges to the Unique Property Discoveries. *Chem. Soc. Rev.* **2012**, *41*, 3594–3623.
13. Jin, R. C.; Zhu, Y.; Qian, H. F. Quantum-Sized Gold Nanoclusters: Bridging the Gap between Organometallics and Nanocrystals. *Chem.—Eur. J.* **2011**, *17*, 6584–6593.
14. Wilcoxon, J. P.; Abrams, B. L. Synthesis, Structure and Properties of Metal Nanoclusters. *Chem. Soc. Rev.* **2006**, *35*, 1162–1194.
15. Shang, L.; Dong, S. J.; Nienhaus, G. U. Ultra-Small Fluorescent Metal Nanoclusters: Synthesis and Biological Applications. *Nano Today* **2011**, *6*, 401–418.
16. Cademartiri, L.; Kitaev, V. On the Nature and Importance of the Transition between Molecules and Nanocrystals: Towards a Chemistry of "Nanoscale Perfection". *Nanoscale* **2011**, *3*, 3435–3446.
17. Pan, Y.; Leifert, A.; Ruau, D.; Neuss, S.; Bornemann, J.; Schmid, G.; Brandau, W.; Simon, U.; Jahnen-Dechent, W. Gold Nanoparticles of Diameter 1.4 nm Trigger Necrosis by Oxidative Stress and Mitochondrial Damage. *Small* **2009**, *5*, 2067–2076.
18. Pan, Y.; Neuss, S.; Leifert, A.; Fischler, M.; Wen, F.; Simon, U.; Schmid, G.; Brandau, W.; Jahnen-Dechent, W. Size-Dependent Cytotoxicity of Gold Nanoparticles. *Small* **2007**, *3*, 1941–1949.
19. Rivera Gil, P.; Oberdörster, G.; Elder, A.; Puntes, V.; Parak, W. J. Correlating Physico-Chemical with Toxicological Properties of Nanoparticles: The Present and the Future. *ACS Nano* **2010**, *4*, 5527–5531.
20. Jimenez, V. L.; Georganopoulou, D. G.; White, R. J.; Harper, A. S.; Mills, A. J.; Lee, D. I.; Murray, R. W. Hexanethiolate Monolayer Protected 38 Gold Atom Cluster. *Langmuir* **2004**, *20*, 6864–6870.
21. Knoppe, S.; Boudon, J.; Dolamic, I.; Dass, A.; Bürgi, T. Size Exclusion Chromatography for Semipreparative Scale Separation of $Au_{38}(SR)_{24}$ and $Au_{40}(SR)_{24}$ and Larger Clusters. *Anal. Chem.* **2011**, *83*, 5056–5061.
22. Al-Somali, A. M.; Krueger, K. M.; Falkner, J. C.; Colvin, V. L. Recycling Size Exclusion Chromatography for the Analysis and Separation of Nanocrystalline Gold. *Anal. Chem.* **2004**, *76*, 5903–5910.
23. Wilcoxon, J. P.; Martin, J. E.; Provencio, P. Size Distributions of Gold Nanoclusters Studied by Liquid Chromatography. *Langmuir* **2000**, *16*, 9912–9920.
24. Liu, F. K. Analysis and Applications of Nanoparticles in the Separation Sciences: A Case of Gold Nanoparticles. *J. Chromatogr., A* **2009**, *1216*, 9034–9047.
25. Wilcoxon, J. P.; Provencio, P. Etching and Aging Effects in Nanosize Au Clusters Investigated Using High-Resolution Size-Exclusion Chromatography. *J. Phys. Chem. B* **2003**, *107*, 12949–12957.
26. Carney, R. P.; Kim, J. Y.; Qian, H. F.; Jin, R. C.; Mehenni, H.; Stellacci, F.; Bakr, O. M. Determination of Nanoparticle Size Distribution Together with Density or Molecular Weight by 2d Analytical Ultracentrifugation. *Nat. Commun.* **2011**, *2*, 8.
27. Planken, K. L.; Colfen, H. Analytical Ultracentrifugation of Colloids. *Nanoscale* **2010**, *2*, 1849–1869.
28. Williams, S. K. R.; Runyon, J. R.; Ashames, A. A. Field-Flow Fractionation: Addressing the Nano Challenge. *Anal. Chem.* **2010**, *83*, 634–642.
29. Lespes, G.; Gigault, J. Hyphenated Analytical Techniques for Multidimensional Characterisation of Submicron Particles: A Review. *Anal. Chim. Acta* **2011**, *692*, 26–41.
30. Hagendorfer, H.; Kaegi, R.; Parlinska, M.; Sinnet, B.; Ludwig, C.; Ulrich, A. Characterization of Silver Nanoparticle Products Using Asymmetric Flow Field Flow Fractionation with a Multidetector Approach—A Comparison to Transmission Electron Microscopy and Batch Dynamic Light Scattering. *Anal. Chem.* **2012**, *84*, 2678–2685.
31. Unrine, J. M.; Colman, B. P.; Bone, A. J.; Gondikas, A. P.; Matson, C. W. Biotic and Abiotic Interactions in Aquatic Microcosms Determine Fate and Toxicity of Ag Nanoparticles. Part 1. Aggregation and Dissolution. *Environ. Sci. Technol.* **2012**, *46*, 6915–6924.
32. Gigault, J.; Hackley, V. Differentiation and Characterization of Isotopically Modified Silver Nanoparticles in Aqueous Media Using Asymmetric-Flow Field Flow Fractionation Coupled to Optical Detection and Mass Spectrometry. *Anal. Chim. Acta* **2012**, 57–66.
33. Kumar, S.; Bolan, M. D.; Bigioni, T. P. Glutathione-Stabilized Magic-Number Silver Cluster Compounds. *J. Am. Chem. Soc.* **2010**, *132*, 13141–13143.
34. Negishi, Y.; Nobusada, K.; Tsukuda, T. Glutathione-Protected Gold Clusters Revisited: Bridging the Gap between Gold(I)−Thiolate Complexes and Thiolate-Protected Gold Nanocrystals. *J. Am. Chem. Soc.* **2005**, *127*, 5261–5270.
35. Negishi, Y.; Takasugi, Y.; Sato, S.; Yao, H.; Kimura, K.; Tsukuda, T. Magic-Numbered Au-*N* Clusters Protected by Glutathione Monolayers (*N*=18, 21, 25, 28, 32, 39): Isolation and Spectroscopic Characterization. *J. Am. Chem. Soc.* **2004**, *126*, 6518–6519.
36. Nilsson, L.; Leeman, M.; Wahlund, K. G.; Bergenståhl, B. Mechanical Degradation and Changes in Conformation of Hydrophobically Modified Starch. *Biomacromolecules* **2006**, *7*, 2671–2679.
37. Heaven, M. W.; Dass, A.; White, P. S.; Holt, K. M.; Murray, R. W. Crystal Structure of the Gold Nanoparticle $[N(C_8H_{17})_4][Au_{25}(SCH_2CH_2Ph)_{18}]$. *J. Am. Chem. Soc.* **2008**, *130*, 3754–3755.

38. Zhu, M.; Aikens, C. M.; Hollander, F. J.; Schatz, G. C.; Jin, R. Correlating the Crystal Structure of a Thiol-Protected Au-25 Cluster and Optical Properties. *J. Am. Chem. Soc.* **2008**, *130*, 5883–5885.
39. Tsunoyama, H.; Tsukuda, T. Magic Numbers of Gold Clusters Stabilized by PVP. *J. Am. Chem. Soc.* **2009**, *131*, 18216–18217.
40. Levard, C. m.; Reinsch, B. C.; Michel, F. M.; Oumahi, C.; Lowry, G. V.; Brown, G. E. Sulfidation Processes of PVP-Coated Silver Nanoparticles in Aqueous Solution: Impact on Dissolution Rate. *Environ. Sci. Technol.* **2011**, *45*, 5260–5266.
41. Schimpf, M.; Caldwell, K.; Giddings, J. C., *Field-Flow Fractionation Handbook*; John Wiley & Sons: New York, 2000.
42. Zhou, R. J.; Shi, M. M.; Chen, X. Q.; Wang, M.; Chen, H. Z. Atomically Monodispersed and Fluorescent Sub-nanometer Gold Clusters Created by Biomolecule-Assisted Etching of Nanometer-Sized Gold Particles and Rods. *Chem.—Eur. J.* **2009**, *15*, 4944–4951.
43. Yu, J.; Patel, S. A.; Dickson, R. M. *In Vitro* and Intracellular Production of Peptide-Encapsulated Fluorescent Silver Nanoclusters. *Angew. Chem., Int. Ed.* **2007**, *119*, 2074–2076.
44. The identification of any commercial product or trade name does not imply endorsement or recommendation by the National Institute of Standards and Technology.
45. MacCuspie, R. I.; Allen, A. J.; Hackley, V. A. Dispersion Stabilization of Silver Nanoparticles in Synthetic Lung Fluid Studied under *In Situ* Conditions. *Nanotoxicology* **2011**, *5*, 140–156.